FULL PAPER

Advanced Energy-Storage Architectures Composed of Spinel Lithium Metal Oxide Nanocrystal on Carbon Textiles

Laifa Shen, Bing Ding, Ping Nie, Guozhong Cao, and Xiaogang Zhang**

Current battery technologies are known to suffer from kinetic problems associated with the solid-state diffusion of Li^+ in intercalation electrodes materials. Not only the use of nanostructure materials but also the design of electrode architectures can lead to more advanced properties. Here, advanced electrode architectures consisting of carbon textiles conformally covered by $Li_4Ti_5O_{12}$ nanocrystal are rationally designed and synthesized for lithium ion batteries. The efficient two-step synthesis involves the growth of ultrathin TiO_2 nanosheets on carbon textiles, and subsequent conversion into spinel $Li_4Ti_5O_{12}$ through chemical lithiation. Importantly, this novel approach is simple and general, and it is used to successfully produce $LiMn_2O_4$/carbon composites textiles, one of the leading cathode materials for lithium ion batteries. The resulting 3D textile electrode, with various advantages including the direct electronic pathway to current collector, the easy access of electrolyte ions, the reduced Li^+/e^- diffusion length, delivers excellent rate capability and good cyclic stability over the Li-ion batteries of conventional configurations.

1. Introduction

High performance energy storage devices with ultrafast charge and discharge rate have been attracting tremendous interest in powering future advanced communication equipment and electric vehicles. Current lithium ion batteries (LIBs) commonly based on layered Co oxide cathode and carbon anode, dominating the portable power market, cannot be matched to the requirement of practical large-scale application because of their low power densities, poor cycling performance, and especially potential safety concerns.[1–4] It is essential to develop advanced materials with desirable electrode architectures that overcome those drawbacks.

L. F. Shen, B. Ding, P. Nie, Prof. X. G. Zhang
College of Materials Science and Engineering
Key Laboratory for Intelligent Nano Materials and Devices of Ministry of Education
Nanjing University of Aeronautics and Astronautics
Nanjing, 210016, PR China
E-mail: azhangxg@nuaa.edu.cn
L. F. Shen, Prof. G. Z. Cao
Department of Materials Science and Engineering
University of Washington
Seattle, WA 98195, USA
E-mail: gzcao@u.washington.edu

DOI: 10.1002/aenm.201300456

Spinel lithium metal oxide with stable three-dimensional (3D) crystal structure possesses fast kinetics because lithium ions can insert from any angle. Compared to commercial graphite anode, spinel $Li_4Ti_5O_{12}$ (LTO) exhibits a relatively high lithium insertion/extraction voltage of approximately 1.55 V (vs. Li/Li^+), which circumvents the formation of the SEI and suppress lithium dendrite deposition on the surface of the anode.[5–7] As a zero-strain insertion material, LTO possesses excellent reversibility in the charge–discharge process.[8,9] As a cathode material, spinel $LiMn_2O_4$ (LMO) is a promising candidate to replace layered Ni or Co oxide materials because of its intrinsic environmental friendliness, low-cost, and high safety.[10–12] For high power application, the electrode materials in LIBs must possess rapid ionic and electronic diffusion. However, the application of LTO (LMO) is hindered by several problems: (i) low electrical conductivity (For example: $S_{LTO} < 10^{-13}$ S cm^{-1});[13–15] (ii) moderate Li^+ diffusion coefficient in the solid lithium metal oxide phase, which implies only a limited area of the outer surface layer would be available for Li^+ insertion/extraction especially at high charge–discharge rates.[16–19]

Approaches for enhancing ion and electron transport kinetics in batteries include tailoring the particle size of electroactive materials[20–23] and enhancing the electronic conductivity with a surface conductive layer.[24–26] Reducing the characteristic dimension of electroactive materials is very effective in improving power performance due to drastically shortened transport distance for ion and electron. In this context, extensive work has focused on synthesizing low-dimensional nanostructured materials (e.g., nanoparticles, nanowires, and nanosheets)[27–29] with high specific surface area and short lithium diffusion length. Nano electroactive materials need to be mixed with polymeric binder and carbon black, and further pressed onto current collector. However, the addition of conductive additive and binder inevitably sacrifices overall energy storage capacity; more importantly, the binder involved will greatly decrease the electrical conductivity of the electrode materials, hindering their potential application in high-performance LIBs. The ideal electrode architecture consisting of 3D highly conductive scaffold coated with nanosized electroactive material would provide efficient ion and electron transport. For example, Braun and co-workers[30] developed a new electrode

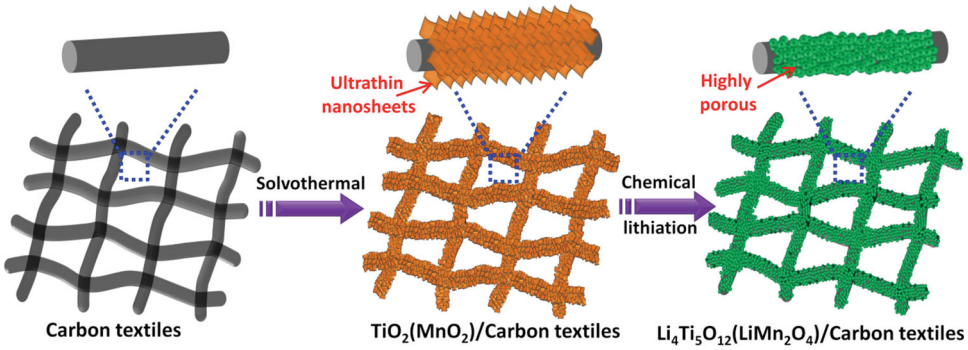

Figure 1. Schematic illustration of the fabrication of binder-free 3D lithium metal oxide/carbon textiles.

using bicontinuous nickel as conductive scaffold, which offer dramatically improved charge and discharge rates for battery. However, due to the potential incompatibility issue between LTO (LMO) and current collector, the direct growth of LTO (LMO) with an optimal particle size and porous structure on current collector still remains very challenging.

In this work, we describe a generally applicable strategy to in-situ grow lithium metal oxide nanocrystals on carbon textiles for the first time, and their formation of 3D flexible lithium metal oxide/carbon composite textiles as intriguing self-supported electrodes for LIBs. The efficient two-step synthesis involves the growth of ultrathin metal oxide nanosheets on the flexible carbon textiles, and subsequent conversion into porous lithium metal oxide nanocrystals through chemical lithiation. The unique binder-free 3D lithium metal oxide/carbon textiles electrode manifests an ultrahigh rate capability and a significantly enhanced cycling performance, suggesting their promising applications in LIBs.

2. Results and Discussion

Figure S1 shows the SEM images of carbon textile templates, which were woven by carbon fibers with high flexibility and high conductivity, making them unique supporting backbones for controlled growth of lithium metal oxide nanocrystals for high power LIBs. The fabrication processes developed in this work are schematically illustrated in **Figure 1**. Firstly, ultrathin TiO_2 nanosheets were grown on the highly flexible carbon textiles through electrostatic interaction under solvothermal condition's. After chemical lithiation and a short post-annealing procedure, TiO_2 nanosheets were transformed in situ into porous LTO nanocrystals to form highly flexible LTO/carbon composite textiles. For comparison, LTO microspheres with an average diameter of ~1 μm were prepared under similar synthesis conditions without use of carbon textiles substrate. Importantly, this novel approach is simple and general, and we have used it to successfully fabricate LMO/carbon composites textiles.

Scanning electron microscopy (SEM) and transmission electron microscopy (TEM) were employed to investigate the morphology and structure of the different materials obtained. **Figure 2**a shows a typical SEM image of TiO_2 nanosheets grown on carbon textiles via solvothermal reaction. The carbon fiber is completely covered with ultrathin TiO_2 nanosheets on its surface. In the high-magnification microscopy images (Figure 2b), the constituent nanosheets are clearly visible and shown to adopt random orientation. These nanosheets with a lateral size of several hundred nanometers are intercrossed with each other, which create loose porous nanostructure with abundant open voids. During the chemical lithiation of TiO_2/carbon

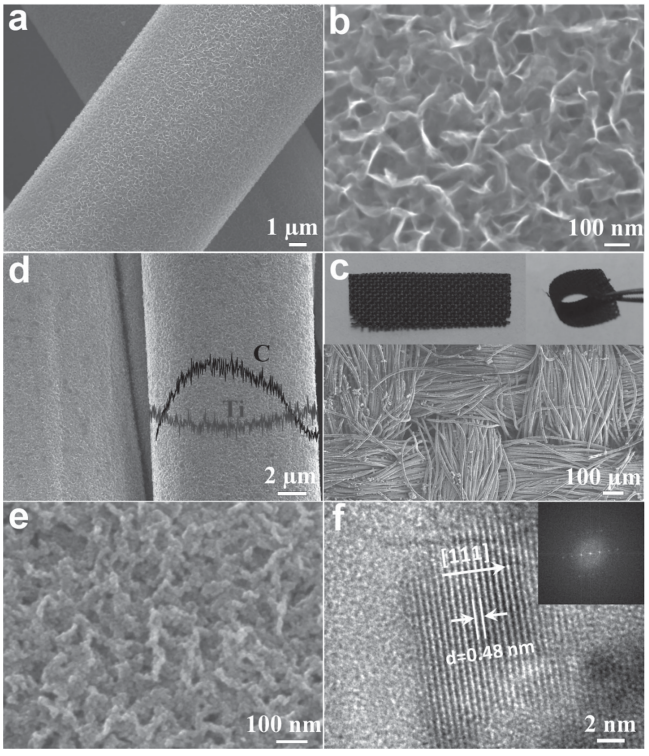

Figure 2. a) Low and b) high magnification SEM images of TiO_2/carbon textiles composite, showing that all the carbon fibers are uniformly coated by ultrathin TiO_2 nanosheets. c,d) Low and e) high magnification SEM images of LTO/carbon textiles composite fabricated by chemical lithiation of TiO_2/carbon textiles, inset shows a digital photograph of a free-standing flexible LTO/carbon textiles electrode. f) HRTEM image of LTO nanocrystals grown on a carbon textiles, inset shows the corresponding FFT patterns.

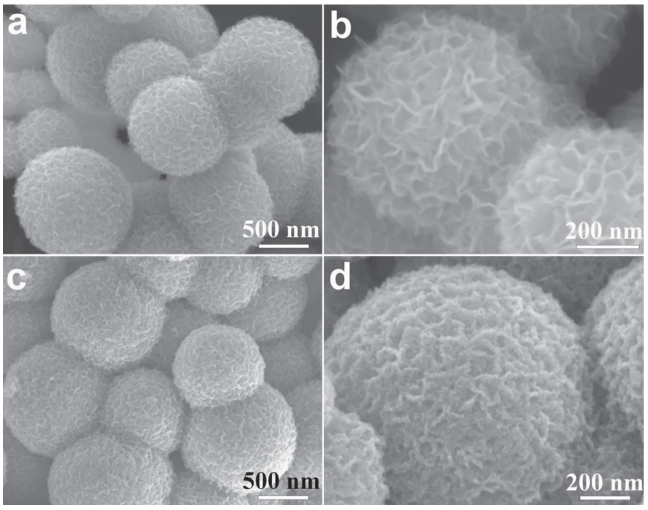

Figure 3. SEM images of a, b) TiO_2 microspheres, c, d) LTO microspheres prepared in the absence of carbon textiles.

textiles in LiOH solution, the nanosheets retracted into particles to reduce the surface energy to produce the LTO/carbon textiles composite. Low SEM image (Figure 2c) of the obtained LTO/carbon textiles reveals a well-established texture structure that preserved the ordered woven structure of the carbon textiles templates. Inset in Figure 2c shows a digital photograph of LTO/carbon textiles electrode that can be folded and flexed, demonstrating the good flexibility. The SEM image in Figure 2d better revealed wormhole-like LTO uniform coated on each carbon fiber to form core/shell structure. EDS line-scanning elemental profiles across a carbon/LTO core/shell fiber are also superimposed in Figure 2d. The C profile showed a peak that was located at the center of the Ti profile. This result directly features the core/shell configuration. The high-magnification SEM image in Figure 2e shows that the ultrathin nanosheets-like structure of TiO_2 precursor almost disappeared but the highly porous curved character were conserved in LTO framework. Not only the carbon textiles are 3D interconnected but the porous shell also exhibits a 3D interconnected framework composed of nanosized building blocks-LTO nanocrystals-with an average size of about 12 nm. Figure 2f shows the TEM image of LTO shell scratched down from the carbon textiles, which clearly reveals that it consists of very small size of the crystals. A lattice spacing of 0.48 nm was observed, in a good agreement with the d-spacing of 0.484 nm associated with the (111) direction of spinel structure (ICDD 00-049-0207). The fast Fourier transform (FFT) pattern taken along the (111) zone axis (inset of Figure 2f) also confirmed the formation of a highly crystallized spinel phase. In comparison, only micrometer-sized TiO_2 spheres with an average size of ~1 μm will be formed under similar synthesis conditions without the addition of carbon textiles substrates (**Figure 3**a). The high-magnification SEM image in Figure 3b clearly reveals that the structure of the microspheres are comprised of many ultrathin nanosheets. After chemical lithiation and a short post-annealing procedure, the TiO_2 spheres were converted to LTO microspheres (Figure 3c, d).

The X-ray diffraction (XRD) patterns of carbon textiles display a typical graphite (002) and (100) reflections at two theta of 26.21 and 43.61, respectively (Figure S2). **Figure 4**a shows the XRD pattern for LTO microspheres, in which all of the diffraction peaks can be assigned to spinel LTO phase (JCPDS Card No. 49-0207). No peaks of the TiO_2 precursor phase and other impurities were detected even though the composite were synthesized at a relatively lower temperature than typical reaction temperature of spinel LTO, suggesting a successful transformation of TiO_2 to LTO. With the exception of the reflections owing to carbon textiles, all peaks in Figure 4b could be indexed to spinel LTO phase. Detailed peak broadening analysis of the (111) XRD reflection using the Scherrer equation indicates that the average crystallite size is approximately 12 nm, which corroborate well with the SEM observation.

In order to identify binder-free 3D architecture is more favorable for high-rate lithium storage, coin-type cell configuration was used to evaluate the electrochemical properties of LTO/carbon textiles, and the results were compared with conventional binder-enriched LTO microsphere electrode prepared by the traditional slurry-coating technique. For binder-enriched LTO microspheres with an average size of 1 μm, the first discharge capacity is 165 mAh g^{-1} at a rate of 1 C (**Figure 5**a). With increasing C rates, the capacities and discharge voltage plateau of LTO microspheres rapidly decrease. For example, the LTO microspheres had no clear discharge voltage plateau and the capacity retention at 60 C was only 34% of the capacity at 1 C, which might be caused by high electrode polarization. At high current densities, an effective utilization of the material is limited only to the outer surface of electrodes. By comparison, the binder-free 3D LTO/carbon textiles composite, in which 12 nm-sized LTO nanoparticles directly grown on carbon microfiber current collector, exhibited greatly improved electrochemical performance (Figure 5b). At a low C-rate of 1 C, the electrode achieved a first discharge capacity as high as 177 mA h g^{-1} (The specific capacity is calculated based on the weight of the LTO), which is a little higher than the theoretical capacity of LTO (175 mA h g^{-1}). Li storage in carbon textile is mainly occurring below 1 V, which can be seen from the charge and discharge curve of carbon textile (Figure S3). The LTO direct connection to the growth substrate improve the electrochemical activity

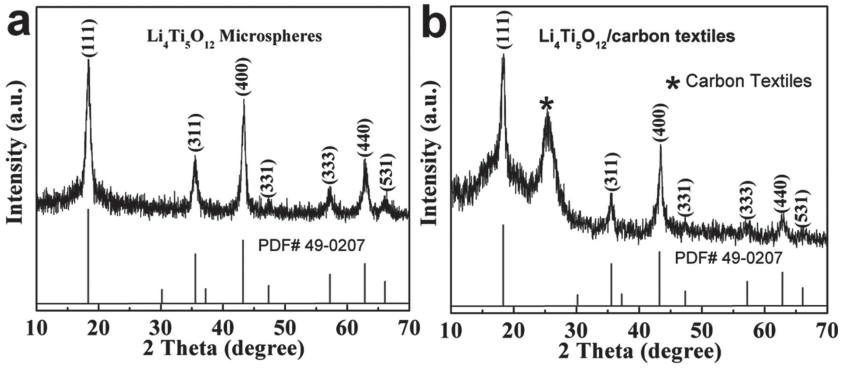

Figure 4. XRD patterns of a) LTO microspheres and b) LTO/carbon textiles composite.

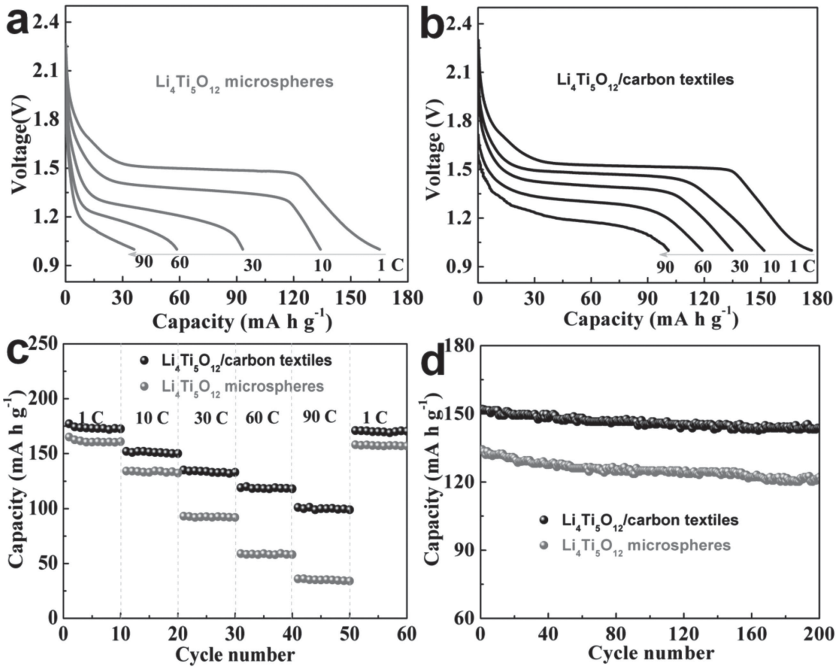

Figure 5. Comparison of electrochemical properties of LTO/carbon textiles composite and LTO microspheres: the discharge curves of a) LTO microspheres and b) LTO/carbon textiles composite. c) Specific discharge capacities at various C rates. d) Cycling performances at the rate of 10 C.

of LTO due to the improved kinetics. In addition, the electrode showed a flat voltage plateau at the potential of 1.52 V ascribable to the redox of Ti^{4+}/Ti^{3+} couple. As the current rate increased from 10, 30 to 60 C, the discharge capacity slightly decreased from 152 to 134 and 119 mAh g^{-1}, respectively. It is very important to note that, even at high rate of 90 C, the potential plateau was still retained and the delivered capacity was still ~58% of the value achieved at 1 C. Figure 5c shows the dependence of the cyclic ability on the rate capabilities with various C rates for two different types of electrode architectures. The discharge specific capacities of the LTO microspheres decrease significantly from 1 to 90 C, whereas the LTO/carbon textiles decrease much more slowly at the same range. It is noteworthy that the discharge capacity obtained in LTO/carbon textiles composite at a high rate of 90 C is higher than that obtained at a rate of 30 C for the LTO microspheres. The reversibility of LTO/carbon textiles composite is demonstrated by the fact that the capacity of 171 mA h g^{-1} is recovered when the current density is reduced back to 1 C. Furthermore, cycling behaviors for the two different electrodes were tested at 10 C and the results are shown in Figure 5d. After 200 cycles the discharge capacity of the LTO microspheres was 121 mA h g^{-1} with 9.2% capacity loss. But for LTO/carbon textiles, the corresponding values were 144 mA h g^{-1} and only 5.3%, respectively, demonstrating that the binder-free 3D architecture effectively enhanced lithium-ion storage capacity and improved storage kinetics, particularly at high C rates.

We also compared this work with other LTO based high-rate electrodes from recent literature,[31–38] and the result shown in **Figure 6**. Ancillary materials such as polymer binder that do not contribute to lithium storage capacity were used in fabrication of traditional LTO-based high rate electrode, resulting in low electrode storage density. For example, TiO_2 nanocoated LTO nanosheets electrode deliver a high capacity of 178 and 161 mA h g^{-1} at 1 C and 10 C, respectively. Taking the total electrode mass (excluding the current collector) into consideration, its capacity deceases to 142 and 129 mA h g^{-1}, respectively. By comparison, the novel binder-free flexible 3D electrode composed of LTO nanocrystals on current collectors of carbon textiles yields much better rate capability than other LTO based high rate electrode.

The configuration of a conventional binder-enriched electrode in Li-ion battery is illustrated in **Figure 7**a. The conventional binder-enriched electrode increase additional undesirable interparticle resistance, more importantly, which failed to provide efficient electron transport between electroactive materials and current collector substrate. The electrochemical reaction path is different in our new concept of 3D flexible electrode consisting of conductive carbon textiles (current collector) conformal coated with LTO nanocrystals (active materials) (Figure 7b): 3D highly electronic conductive of carbon textiles proved an expressway for charge transfer; loose textures and open spaces between neighboring carbon fibers making more active material exposed to the electrolyte that facilitate the fast transfer of Li^+; The nano-sized active materials shortens the Li^+ and e^- diffusion paths, avoiding the use of binders or any conducting additive material in this unique electrode architecture. All of these could be ensure the effective ambipolar diffusion of Li^+ and e^- into/out of 3D flexible electrode architecture, enabling remarkable rate capability and cycling performance.

The feature of this unique electrode architecture for fast lithum storage is also confirmed in the binder-free 3D LMO/carbon textiles electrode. Ultrathin MnO_2 nanosheets were uniformly grown on carbon textiles surface via a redox reaction between $KMnO_4$ and carbon under hydrothermal condition

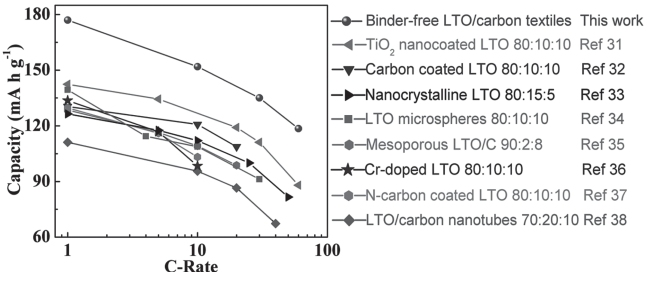

Figure 6. Comparison of rate capability of binder-free 3D LTO/carbon textiles electrode with other LTO based high-rate electrodes reported recently. The capacities were estimated based on their total mass of electrode material. Their electrode compositions are listed using the mass ratio of active materials: conductive carbon: binder.

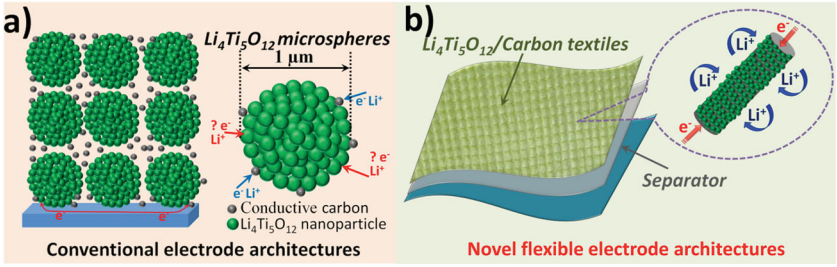

Figure 7. Schematic drawing of a) the conventional electrode and b) novel binder-free flexible 3D electrode.

(Figure S4a,b). Then, carbon textiles-supported LMO nanocrystals were in situ formed by chemical lithiation of MnO_2 in LiOH aqueous solution (Figure S4c,d). The LMO/carbon textiles yielded a reversible specific capacity of 124 mA h g^{-1} at 1 C and an exceptional rate-capability of 82% and 69% capacity retention (102 mA h g^{-1} and 85 mA h g^{-1}) at discharge rates of 10 C and 20 C, respectively, thereby indicating its high power performance (Figure S5a,b). The rate performance of LMO/carbon textiles electrode is better than the best nanostructured or hybrid LMO electrodes reported so far (Figure S5c). Cycling data at the 4 C rate for 200 cycles confirms the superior cyclic stability of the LMO/carbon textiles electrode (only ~8% capacity loss; Figure S5d).

3. Conclusions

In summary, a general strategy for the fabrication of binder-free flexible lithium metal oxide/carbon textiles composite with remarkable lithium storage has been demonstrated. The synthesis involves the growth of ultrathin metal oxide nanosheets on the flexible carbon textiles support and subsequently transformed in situ into porous lithium metal oxide nanocrystals through chemical lithiation. Carbon textiles not only support active materials but also serve as current collector, which proved an expressway for charge transfer and eliminated the use of ancillary conducting material and binder. With the high electrical conductivity of the composite, the easy access of electrolyte ions and the reduced Li^+/e^- diffusion length, the novel LTO/carbon textiles electrode possessed rapid ionic and electronic diffusion, enabling excellent rate capability (103 mAh g^{-1} at 90 C) and good cyclic stability (only 5.3% capacity loss after 200 cycles at a rate of 10 C). These important findings could open up new opportunities in constructing high-performance batteries for large-scale wearable energy storage.

4. Experimental Section

Synthesis of LTO/Carbon Textiles: Carbon textiles was refluxed in 6 M HNO_3 solution for 10 h at 80 °C, cleaned by ultrasonically in deionized (DI) water and then dried in a oven. Ultrathin TiO_2 nanosheets grown on carbon textiles by a solvothermal method reported by Lou's group with minor modifications.[39] 5 μL of diethylenetriamine was added to 7 mL of isopropyl alcohol. After gentle stirring for 2 min, 0.1 mL of titanium (IV) isopropoxide (TIP; 97%, Sigma-Aldrich) was added. After putting a piece of carbon cloth (2 cm × 4 cm), the solution was then transferred to a Teflon-lined stainless steel autoclave and kept at 200 °C for 20 h. After hydrothermal growth, the carbon textiles covered with TiO_2 nanosheets was taken out and immersed in 2 M LiOH solution at 60 °C for 8 h. After rinsing with copious amounts of DI water and drying at 60 °C in a oven, the carbon textiles covered with L-T-O (LTO precursor) was calcined in Ar at 550 °C for 2 h to obtain the LTO nanocrystals on carbon textiles. LTO microspheres were also prepared in a similar manner without use of carbon textiles.

Synthesis of LMO/Carbon Textiles: A piece of acid-treated carbon cloth (2 cm × 4 cm) was put into a Teflon-lined stainless steel autoclave containing a 0.03 M $KMnO_4$ solution and then keep at 160 °C for 5 h. After the hydrothermal growth, the carbon textiles covered with MnO_2 nanosheets was taken out and rinsing with DI water. The dried MnO_2/carbon textiles was immersed into 0.08 M LiOH solution, then transferred to a 20 mL Teflon-lined stainless steel autoclave and maintained at 180 °C for 12 h. Finally, the sample was taken out, washed with distilled water, and dried at 60 °C to obtain a flexible LMO/carbon textiles.

Materials Characterization: The crystal structure of the obtained samples was characterized by X-ray diffraction (XRD) (Bruker D8 advance) with Cu Kα radiation. The microstructural properties were characterized using transmission electron microscopy (TEM, JEOL JEM-2010), and scanning electron microscopy (SEM, JEOL, JSM-7000).

Electrochemical Measurement: Electrochemical characterization was performed in coin type cells, which were assembled in an argon-filled glove box using the LTO/carbon textiles (LMO/carbon textiles) assembly as the work electrode and Li metal as the counter and reference electrode. The loading amount of the LTO (LMO) were determined by cutting the carbon textile and LTO (LMO)/carbon textile into smaller pieces with the diameter of 12 mm. Then both the carbon textile and LTO (LMO)/carbon textile were weighed with a high-precision analytical balance (Sartorius, max weight 5100 mg, d = 0.001 mg) from which the exact mass of the samples was then determined. The conventional electrode was prepared by mixing 80 wt% active material (LTO microspheres), 12 wt% carbon black, and 8 wt% polyvinylidene fluoride (PVDF) in N-methyl pyrrolidinone (NMP). The slurry was then spread uniformly on Cu foil current collector and dried under vacuum at 110 °C for 12 h. 1 M $LiPF_6$ solution in a 1: 1 (V: V) mixture of ethylene carbonate (EC) and dimethyl carbonate (DMC) was used as electrolyte. Finally, the cells were then aged for 12 h before measurements. The cells were galvanostatically charged and discharged using an Arbin Battery Tester BT-2000 (Arbin Instruments, College Station, Texas).

Supporting Information

Supporting Information is available from the Wiley Online Library or from the author.

Acknowledgements

This work was supported by the National Natural Science Foundation of China (No. 21173120), the Natural Science Foundation of Jiangsu Province (BK2011030) and the National Science Foundation of the U.S. (CMMI-1030048). L. F. Shen also thanks the Outstanding Doctoral Dissertation in NUAA (BCXJ11-10) for financial support.

Received: April 28, 2013
Revised: June 4, 2013
Published online: June 28, 2013

[1] B. Dunn, H. Kamath, J. Tarascon, *Science* **2011**, *334*, 928.
[2] J. Liu, J. G. Zhang, Z. G. Yang, J. P. Lemmon, C. Imhoff, G. L. Graff, L. Li, J. Hu, C. Wang, J. Xiao, G. Xia, V. V. Viswanathan, S. Baskaran, V. Sprenkle, X. Li, Y. Shao, B. Schwenzer, *Adv. Funct. Mater.* **2012**, *23*, 929.
[3] L. Shen, E. Uchaker, X. Zhang, G. Cao, *Adv. Mater.* **2012**, *24*, 6502.
[4] Z. Chen, D. Zhang, X. Wang, X. Jia, F. Wei, H. Li, Y. Lu, *Adv. Mater.* **2012**, *24*, 2030.
[5] E. Ferg, R. J. Gummow, A. Dekock, M. M. Thackeray, *J. Electrochem. Soc.* **1994**, *141*, L147.
[6] L. Shen, C. Yuan, H. Luo, X. Zhang, K. Xu, Y. Xia, *J. Mater. Chem.* **2010**, *20*, 6998.
[7] M. R. Jo, K. M. Nam, Y. Lee, K. Song, J. T. Park, Y. M. Kang, *Chem. Commun.* **2011**, *47*, 11474.
[8] K. Nakahara, R. Nakajima, T. Matsushima, H. Majima, *J. Power Sources* **2003**, *117*, 131.
[9] Z. Chen, I. Belharouak, Y. K. Sun, K. Amine, *Adv. Funct. Mater.* **2012**, *23*, 959.
[10] F. Jiao, J. Bao, A. H. Hill, P. G. Bruce, *Angew. Chem.* **2008**, *120*, 9857.
[11] F. Cheng, H. Wang, Z. Zhu, Y. Wang, T. Zhang, Z. Tao, J. Chen, *Energy Environ. Sci.* **2011**, *4*, 3668.
[12] X. Jia, C. Yan, Z. Chen, R. Wang, Q. Zhang, L. Guo, F. Wei, Y. F. Lu, *Chem. Commun.* **2011**, *47*, 9669.
[13] Y. K. Sun, S. T. Myung, B. C. Park, J. Prakash, I. Belharouak, K. Amine, *Nat. Mater.* **2009**, *8*, 320.
[14] N. Li, Z. Chen, W. Ren, F. Li, H. M. Cheng, *Proc. Natl. Acad. Sci. USA* **2012**, *109*, 17360.
[15] L. Shen, C. Yuan, H. Luo, X. Zhang, S. Yang, X. Lu, *Nanoscale* **2011**, *3*, 572.
[16] G. N. Zhu, H. J. Liu, J. H. Zhuang, C. X. Wang, Y. G. Wang, Y. Y. Xia, *Energy Environ. Sci.* **2011**, *4*, 4016.
[17] W. J. H. Borghols, M. Wagemaker, U. Lafont, E. M. Kelder, F. M. Mulder, *J. Am. Chem. Soc.* **2009**, *131*, 17786.
[18] L. Shen, H. Li, E. Uchaker, X. Zhang, G. Cao, *Nano Lett.* **2012**, *12*, 5673.
[19] Z. S. Hong, M. D. Wei, T. B. Lan, L. Jiang, G. Cao, *Energy Environ. Sci.* **2012**, *5*, 5408.
[20] K. Amine, I. Belharouak, Z. Chen, T. Tran, H. Yumoto, N. Ota, S. T. Myung, Y. K. Sun, *Adv. Mater.* **2010**, *22*, 3052.
[21] L. Shen, X. Zhang, H. Li, C. Yuan, G. Cao, *J. Phys. Chem. Lett.* **2011**, *2*, 3096.
[22] R. B. Rakhi, W. Chen, D. Cha, H. N. Alshareef, *Nano Lett.* **2012**, *12*, 2559.
[23] S. Lee, Y. Cho, H. K. Song, K. T. Lee, J. Cho, *Angew. Chem. Int. Ed.* **2012**, *124*, 8878.
[24] H. Pan, L. Zhao, Y. S. Hu, H. Li, L. Q. Chen, *ChemSusChem* **2012**, *5*, 526.
[25] K. S. Park, A. Benayad, D. J. Kang, S. G. Doo, *J. Am. Chem. Soc.* **2008**, *130*, 14930.
[26] L. Shen, C. Yuan, H. Luo, X. Zhang, L. Chen, H. Li, *J. Mater. Chem.* **2011**, *21*, 14414.
[27] J. M. Feckl, K. Fominykh, M. Doblinger, D. Fattakhova-Rohlfing, T. Bein, *Angew. Chem. Int. Ed.* **2012**, *51*, 7459.
[28] J. Kim, J. Cho, *Electrochem. Solid-State Lett.* **2007**, *10*, A81.
[29] Y. Liu, W. Zhang, Y. Zhu, Y. Luo, Y. Xu, A. Brown, J. N. Culver, C. A. Lundgren, K. Xu, Y. Wang, C. Wang, *Nano Lett.* **2013**, *13*, 293.
[30] H. Zhang, X. Yu, P. V. Braun, *Nat. Nanotechnol.* **2011**, *6*, 277.
[31] Y. Wang, L. Gu, Y. G. Guo, H. Li, X. He, S. Tsukimoto, Y. Ikuhara, L. J. Wan, *J. Am. Chem. Soc.* **2012**, *134*, 7874.
[32] B. Li, C. Han, Y. He, C. Yang, H. D. Du, Q. H. Yang, F. Y. Kang, *Energy Environ. Sci.* **2012**, *5*, 9595.
[33] A. S. Prakash, P. Manikandan, K. Ramesha, M. Sathiya, J. M. Tarascon, A. K. Shukla, *Chem. Mater.* **2010**, *22*, 2857.
[34] Y. F. Tang, L. Yang, Z. Qiu, J. S. Huang, *J. Mater. Chem.* **2009**, *19*, 5980.
[35] L. Shen, X. Zhang, E. Uchaker, C. Yuan, G. Cao, *Adv. Energy Mater.* **2012**, *2*, 691.
[36] H. Song, S. W. Yun, H. H. Chun, M. G. Kim, K. Y. Chung, H. S. Kim, B. W. Chod, Y. T. Kim, *Energy Environ. Sci.* **2012**, *5*, 9903.
[37] L. Zhao, Y. S. Hu, H. Li, Z. Wang, L. Q. Chen, *Adv. Mater.* **2011**, *23*, 1385.
[38] L. Shen, C. Yuan, H. Luo, X. Zhang, K. Xu, F. Zhang, *J. Mater. Chem.* **2011**, *21*, 761.
[39] J. S. Chen, Y. L. Tan, C. M. Li, Y. L. Cheah, D. Y. Luan, S. Madhavi, F. Y. C. Boey, L. A. Archer, X. W. Lou, *J. Am. Chem. Soc.* **2010**, *132*, 6124.